ภาคผนวก 2

Reprint

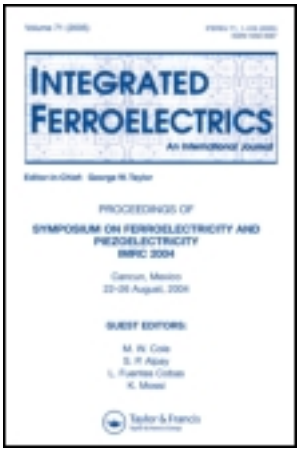

Integrated Ferroelectrics: An International Journal
Publication details, including instructions for authors and subscription information:
http://www.tandfonline.com/loi/ginf20

Effect of Sintering Temperature of Lead-free $(K_{0.50}Na_{0.46}Li_{0.04})(Nb_{(0.96-x)}Sb_{0.04}Ta_x)O_3$ Ceramics on Piezoelectric Properties

Chunmanus Uthaisar [a c], Puripat Kantha [a c], Rattikorn Yimnirun [b c] & Soodkhet Pojprapai [a c]

[a] School of Ceramic Engineering, Institute of Engineering, Suranaree University of Technology, Nakhon Ratchasima, 30000, Thailand

[b] School of Physics, Institute of Science, Suranaree University of Technology and NANOTECH-SUT Center of Excellence on Advanced Functional Nanomaterials, Nakhon Ratchasima, 30000, Thailand

[c] Smart Materials and Intelligent System Research Unit, Suranaree University of Technology, Nakhon Ratchasima 30000, Thailand

Published online: 07 Dec 2013.

To cite this article: Chunmanus Uthaisar, Puripat Kantha, Rattikorn Yimnirun & Soodkhet Pojprapai (2013) Effect of Sintering Temperature of Lead-free $(K_{0.50}Na_{0.46}Li_{0.04})(Nb_{(0.96-x)}Sb_{0.04}Ta_x)O_3$ Ceramics on Piezoelectric Properties, Integrated Ferroelectrics: An International Journal, 149:1, 114-120, DOI: 10.1080/10584587.2013.853588

To link to this article: http://dx.doi.org/10.1080/10584587.2013.853588

Integrated Ferroelectrics, 149:114–120, 2013

ISSN: 1058-4587 print / 1607-8489 online
DOI: 10.1080/10584587.2013.853588

Effect of Sintering Temperature of Lead-free $(K_{0.50}Na_{0.46}Li_{0.04})(Nb_{(0.96-x)}Sb_{0.04}Ta_x)O_3$ Ceramics on Piezoelectric Properties

CHUNMANUS UTHAISAR,[1,3] PURIPAT KANTHA,[1,3] RATTIKORN YIMNIRUN,[2,3] AND SOODKHET POJPRAPAI[1,3,*]

[1]School of Ceramic Engineering, Institute of Engineering, Suranaree University of Technology, Nakhon Ratchasima 30000, Thailand
[2]School of Physics, Institute of Science, Suranaree University of Technology and NANOTECH-SUT Center of Excellence on Advanced Functional Nanomaterials, Nakhon Ratchasima 30000, Thailand
[3]Smart Materials and Intelligent System Research Unit, Suranaree University of Technology, Nakhon Ratchasima 30000, Thailand

Currently, lead-free piezoelectric ceramics are being investigated to replace lead-contained piezoelectric ceramics such as PZT. In this work, the effect of sintering temperature on piezoelectric properties of $(K_{0.50}Na_{0.46}Li_{0.04})(Nb_{(0.96-x)}Sb_{0.04}Ta_x)O_3$ ceramics, where $x = 0$, and 0.12, (KNN-LST) was studied. KNN-LST ceramics were synthesized by the solid state method and sintered at different sintering temperatures (1000–1200°C) for 4 h in a normal atmospheric pressure. It was found that there was different optimum sintering temperatures for each composition. The samples sintered at the optimum sintering temperatures exhibited relatively high density and piezoelectric constant (d_{33}).

Keywords Lead-free piezoelectric; ferroelectric, KNN-LST ceramic; sintering temperature

1. Introduction

Lead-contained piezoelectric ceramics such as lead zircronate titanate (PZT) are the most widely used for transducer and actuator applications because they exhibit excellent piezoelectric properties [1–2]. However, these ceramics are toxic to the body and the environment. Therefore, many researchers is trying to development lead-free piezoelectric ceramics such as BNT, NT, KNN and BT ceramics of which the piezoelectric properties are equivalent to or better than such lead-based piezoelectric ceramics. One of the most interesting lead-free piezoelectric ceramics is potassium sodium niobate ($K_{0.5}N_{0.5}NbO_3$) based ceramics. It was reported that $K_{0.5}N_{0.5}NbO_3$ has a piezoelectric charge constant, d_{33}, of 80–120 pC/N [4–7]. Recently, exceptionally high piezoelectric properties were reported in the $(K,Na)NbO_3$–$LiTaO_3$–$LiSbO_3$ system by Y. Saito et al. [3]. They reported that such KNN based ceramics, which is prepared by a complex processing method, exhibit d_{33} values over 400 pC/N. Moreover, high piezoelectric charge constant $d_{33} > 200$ pC/N has been reported

Received December 9, 2012; in final form August 25, 2013.
*Corresponding author. E-mail: soodkhet@sut.ac.th

for modified $K_{0.5}N_{0.5}NbO_3$ with lithium, antimony, tantalum, barium and titanium dopant [4–12]. It was found that the substitution of such dopants at the A and B sites of the ABO_3 perovskite structure can improve densification and piezoelectric properties of KNN based ceramics [4–7]. In addition to the dopants, the fabrication process such as pressing/forming, calcination, and sintering is one of the keywords to improve the piezoelectric properties of the ceramics.

The aim of this work is to study the relationship between the microstructure, crystal structure and the piezoelectric and dielectric properties as a function of the sintering temperature for modified KNN piezoelectric ceramics of the (Na, K, Li)(Nb, Ta, Sb)O_3 system.

2. Experimental

KNN-LST $(K_{0.50}Na_{0.46}Li_{0.04})(Nb_{(0.96-x)}Sb_{0.04}Ta_x)O_3$ (x = 0, 0.12) and KNN-N ($K_{0.52}N_{0.46}NbO_3$) were synthesized by solid state reaction. They were prepared from Nb_2O_5 (99.90%), Na_2CO_3 (99.90%), K_2CO_3 (99.00%), $LiCO_3$ (98.50.%), Sb_2O_5 (99.995%) and Ta_2O_5 (99.99%) respectively. To obtain the homogeneous powder particles, each oxide powder was milled 24 hr in ethanol. Then the powder was dried in an oven at 180°C to remove the ethanol. After drying, it was ground and sieved to obtain the finer particle. Each oxide powder was mixed by using wet milling 24 hr in ethanol. This homogeneous powder was put into a crucible and then calcined at 850°C for 6 h. After that, the powder was mixed with PVA 5%wt. and sieved by using a 425 μm (120 mesh) sieve. The powder was formed into disk shape with diameter of 12 mm and thickness of 1 mm by using a uniaxial hydraulic pressing machine (CARVER) at 130 MPa and cold isostatic pressing machine (Avure Technologies Inc. LCIP22260) at 250 MPa. The samples, then, were sintered at 1000–1200°C at normal atmospheric pressure for 4 h. with heating/cooling rate of 5°C/min. For electrical properties measurement, the sintered KNN-N and KNN-LST samples were ground and polished by using 1800-grit to 2000-grit sandpaper. The polished samples with a diameter of 10 mm and thickness of 1 mm were coated by gold electrodes using a sputtering machine (JEOL-JFC-1100E). The samples sintered at 1130°C were poled along the thickness direction at 200°C in a silicon oil bath under a DC electric field of 2.5 kV/mm for 30 min while those sintered at 1000 and 1200°C were poled at 2.0 kV/mm. It is noted that the later samples broke down when the poling field exceeded 2.0 kV/mm.

Crystal structures of the sintered sample were characterized by X-ray diffraction technique (XRD) (BLUKER AXS-D5005). The microstructure of the sintered samples was observed by a scanning electron microscope (SEM) (JEOL-5800). The bulk density was measured by Archimedes method at room temperature. The piezoelectric constant; d_{33} was measured at room temperature using a quasi-static method by a piezo-d_{33} meter (APC product inc. S5865). The room temperature dielectric constant was carried out at 100 kHz using an LCR meter (GW INSTEK LCR-821).

3. Result and Discussion

Figure 1 shows the X-ray diffraction (XRD) patterns of (a) KNN-N, (b) KNN-LS and (c) KNN-LST12 ceramics which are sintered at 1000°C, 1130°C and 1200°C.. All XRD pattern indicated that the samples show perovskite structure. The second phase $K_3Li_2Nb_5O_{15}$ was observed around $2\theta \sim 26$–30° and was indexed by using the JCPDS pattern (034-0122) [5].

Figure 2 shows the XRD patterns in the ranges of 44° to 47° and 55° to 58°. All XRD patterns obtained from KNN-N represent orthorhombic phase as shown in

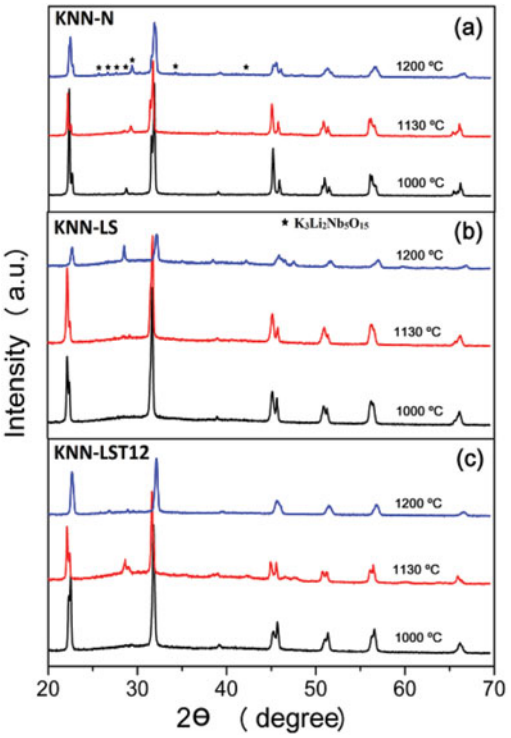

Figure 1. XRD patterns of (a) KNN-N, (b) KNN-LS and (c) KNN-LST12 ceramics with varying sintering temperature. (Color figure available online.)

Fig. 2(a–b). XRD of KNN-LS sintered at 1000 and 1130°C exhibits mixture of orthorhombic and tetragonal phase while those samples sintered at 1200°C shows orthorhombic phase (see Fig. 2(c-d)). XRD patterns of KNN-LST12 sintered at 1000°C, 1130°C, and 1200°C represents tetragonal, mixture of orthorhombic, and tetragonal phase, respectively (see Fig. 2(e–f)). The orthorhombic and tetragonal phase was indexed by using the JCPDS pattern 071-271 and 071–0945, respectively. It is noticed that the XRD patterns obtained from the samples sintered at 1200°C exhibits broad peak which could be attributed to the grain size effect which is evidenced by micrographs in Fig. 3.

Figure 3(a–c) shows the scanning electron micrographs of ceramics sintered at 1000°C. From this figure, it can be seen that the chemical reaction may not be complete to form a crystal structure. On the other hand, the microstructure of ceramics sintered at 1130°C and 1200°C show more clear crystal structure compared to the samples sintered at 1000°C (see Fig. 4(a–f)). KNN-N sintered at 1130°C has fine grains (∼5 μm) while the ceramic sintered at 1200°C has coarse grains (∼15 μm). This can be a result of grain growth due to an increasing of sintering temperature. The KNN-LS sintered at 1130°C has fine grains (∼5 μm) (see Fig. 4(c)) while the ceramic sintered at 1200°C has coarse grains (∼7μm) (see Fig. 4(d)). KNN-LST12 sintered at 1130°C has fine grains (∼1–3 μm) (see Fig. 4(e)) while the ceramic sintered at 1200°C has coarse grains (∼5–6 μm) (see Fig. 4(f)). The smallest grain size was found in the sintered KNN-LST12 samples when compared with other composition. This indicates that the addition of Li, Sb and Ta are affected on the grain size of KNN ceramics [13]. Not only that, a bimodal distribution was clearly found

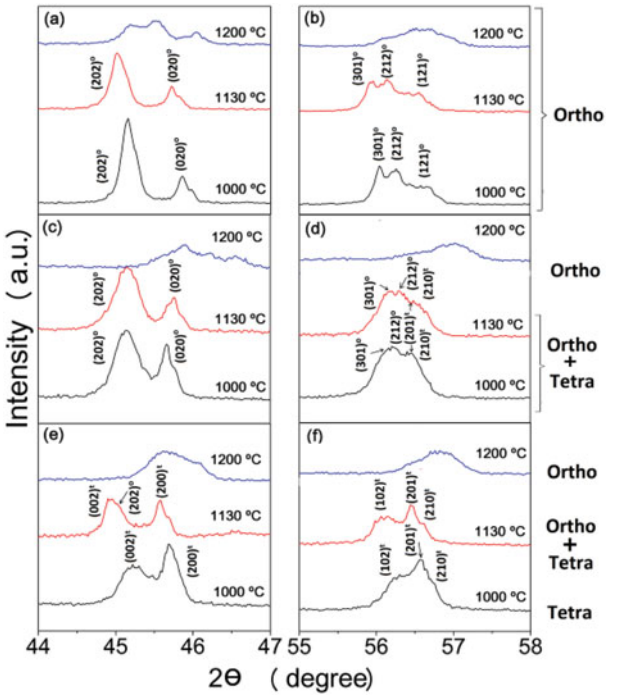

Figure 2. XRD patterns of (a–b) KNN-N, (c–d) KNN-LS and (e–f) KNN-LST12 ceramics showing a phase transition for $2\theta = 44$–47° and 55–58°. (Color figure available online.)

continuously with increasing Ta content. It is probably due to the larger ionic radius Ta^{5+} substitute into Nb^{5+} site, leading to the distortion of crystal structure [14].

Figure 5(a) shows the bulk densities of KNN-N, KNN-LS and KNN-LST12 as a function of sintering temperature. The density of all samples increase with increasing sintering temperature up to 1130°C, and then decrease further temperature higher. The maximum density of KNN-N, KNN-LS and KNN-LST12 were 3.72 g/cm^3, 4.28 g/cm^3 and 4.41 g/cm^3, respectively for sintered ceramics at 1130°C. From this result, it was also found that the density of all sintered KNN-LST12 samples were higher than KNN-N and KNN-LS samples. This clarifies that the Ta doping and sintering temperature can improve the density of samples.

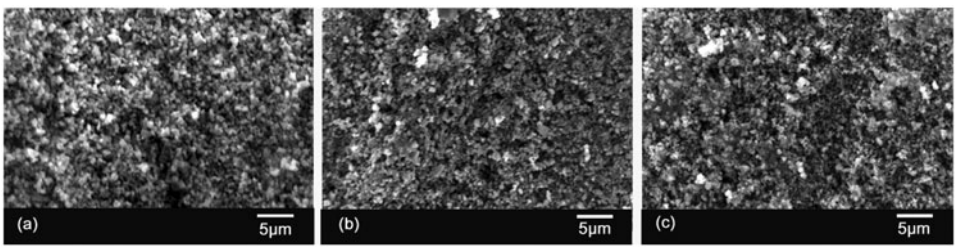

Figure 3. Scanning electron micrographs of (a) KNN-N, (b) KNN-LS and (c) KNN-LST12 ceramics sintered at 1000°C.

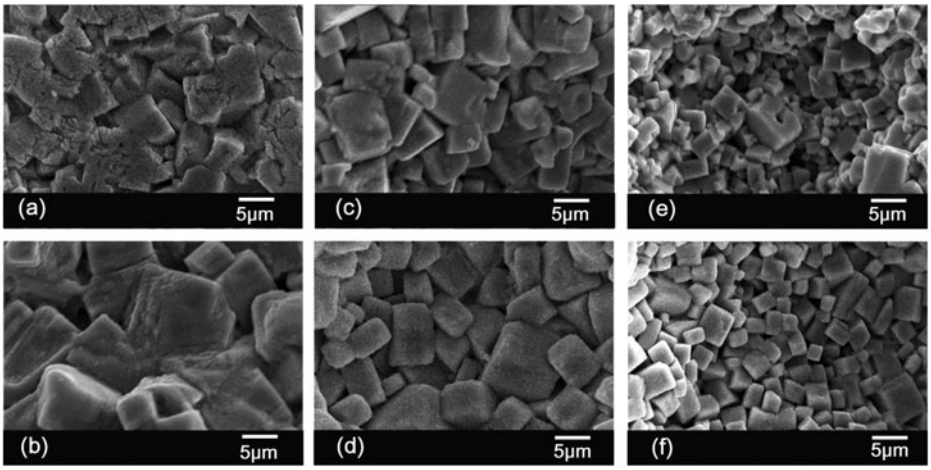

Figure 4. Scanning electron micrographs of (a, b) KNN-N, (c, d) KNN-LS and (c, f) KNN-LST12 ceramics sintered at 1130°C and 1200°C, respectively.

Figure 5(b) shows the piezoelectric charge constant (d_{33}) of all sintered samples as a function of sintering temperature. KNN-N ceramics show a maximum d_{33} of ∼83 pC/N for sintered 1130°C sample, while KNN-LS and KNN-LST12 ceramics show ∼133 and ∼192 pC/N, respectively as the same sintering temperature. The d_{33} value is related to the

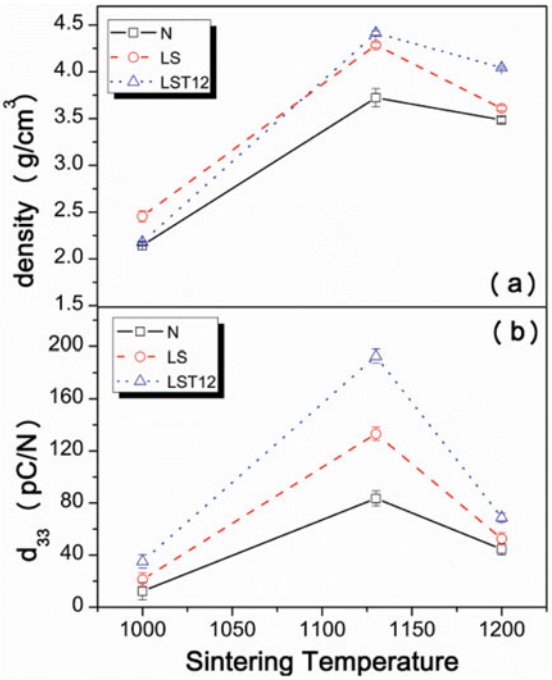

Figure 5. (a) Bulk densities, (b) d_{33} of KNN-N, KNN-LS and KNN-LST12 as a function of sintering temperature. (Color figure available online.)

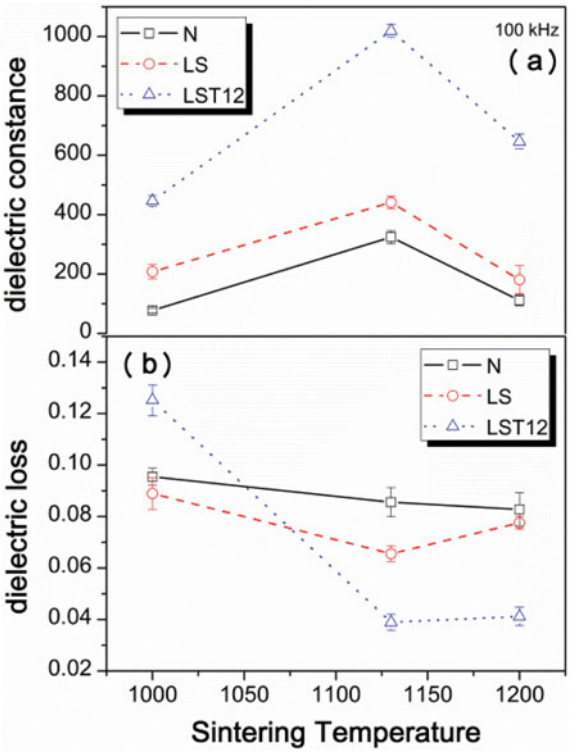

Figure 6. (a) Room temperature dielectric constant (ε_r) and (b) dielectric loss ($tan\delta$) of KNN-N, KNN-LS and KNN-LST12 as a function of sintering temperature. (Color figure available online.)

bulk density as shown in Fig. 5(a–b), which maximum value of those found at 1130°C. However, the sintering temperature increases to 1200°C, d_{33} value of all compositions decreased. The same tends was found in the room temperature dielectric constant (ε_r) (see Fig. 6). A maximum value of the dielectric constant (ε_r) ∼1019 with the lowest dielectric loss ($tan\delta$) ∼0.038 was found for KNN-LST12 ceramics sintered at 1130°C. Therefore, the 12% Ta doped and sintered at 1130°C sample was selected as optimum composition.

4. Conclusion

In this work, all ceramic samples were produced by solid-state reaction method. The optimum sintering temperature for prepare the KNN-N, KNN-LS and KNN-LST12 ceramics is 1130°C for 4 h. The crystal structure of ceramic samples was perovskite structure with different symmetry. KNN-N samples only represent orthorhombic phase while KNN-LS and KNN-LST12 ceramics represent the mixture of orthorhombic and tetragonal phase. The density of all ceramics increases with increasing sintering temperature and Ta content. The KNN-LST12 was found to be the best of all samples due to it showed maximum piezoelectric constant d33 (∼192 pC/N) and dielectric constant (∼1019) with low dielectric loss (∼0.038). This result indicates that the optimum sintering temperature and Ta addition develops the dielectric and piezoelectric properties of KNN-based ceramics.

Acknowledgments

This project is supported by Thai Research Fund (TRF5680095). S. Pojprapai would like to thank Associate Professor Dr. Jurassri and Dr. Veerayuth Lorprayoon for their kind support.

References

1. Y. Chang, Z. Yang, L. Wei *et al.* , Effects of $AETiO_3$ (AE = Mg, Ca, Sr, Ba) additions on phase structure, microstructure and electrical properties of $(K_{0.5}Na_{0.5})$ NbO_3 ceramics. *Materials Science and Engineering: A.* **437**, 2, 301–305, (2006).
2. F. Rubio-Marcos, P. Ochoa, and J. Fernandez, Sintering and properties of lead-free (K, Na, Li)(Nb, Ta, Sb) O_3 ceramics. *Journal of the European Ceramic Society.* **27**, 13–15, 4125–4129, (2007).
3. Y. Saito, H. Takao, T. Tani *et al.* , Lead-free piezoceramics. *Nature.* **432**, 7013, 84–87, (2004).
4. R. Muanghlua, S. Niemcharoen, M. Sutapun *et al.* , Phase transition behaviour and electrical properties of lead-free $(K_{0.5}Na_{0.5})$ NbO_3-$LiNbO_3$-$LiSbO_3$ piezoelectric ceramics. *Current Applied Physics.* **11**, 3, 434–437, (2011).
5. W. Liang, D. Xiao, W. Wu *et al.* , Effect of sintering temperature on phase transitions, properties and temperature stability of $(K_{0.465}Na_{0.465}Li_{0.07})(Nb_{0.95}Sb_{0.05})$ O_3 lead-free piezoelectric ceramics. *Current Applied Physics*, 2011.
6. E. Hollenstein, D. Damjanovic, and N. Setter, Temperature stability of the piezoelectric properties of Li-modified KNN ceramics. *Journal of the European Ceramic Society.* **27**, 13–15, 4093–4097, (2007).
7. K. Higashide, K. Kakimoto, and H. Ohsato, Temperature dependence on the piezoelectric property of (1-x)$(Na_{0.5}K_{0.5})$ NbO_3-x$LiNbO_3$ ceramics. *Journal of the European Ceramic Society.* **27**, 13–15, 4107–4110, (2007).
8. J. H. Cho, Y. H. Lee, and B. I. Kim, Domain structure of orthorhombic (Li, K, Na) NbO_3 ceramics. *Journal of Ceramic Processing Research.* **11**, **2**, 237–240, (2010).
9. H. Du, F. Tang, F. Luo *et al.* , Influence of sintering temperature on piezoelectric properties of $(K_{0.5}Na_{0.5})$ NbO_3-$LiNbO_3$ lead-free piezoelectric ceramics. *Materials research bulletin.* **42**, 9, 1594–1601, (2007).
10. Y. Guo, K. Kakimoto, and H. Ohsato, Phase transitional behavior and piezoelectric properties of (NaK) NbO–LiNbO ceramics. *Applied physics letters.* **85**, 4121, (2004).
11. G. Z. Zang, J. F. Wang, H. C. Chen *et al.* , Perovskite $(Na_{0.5}K_{0.5})_{1-x}(LiSb)_xNb_{1-x}O_3$ lead-free piezoceramics. *Applied physics letters.* **88**, 21, 212908-212908-3, (2006).
12. Y. Dai, and X. Zhang, Phase transition behavior and electrical properties of lead-free (1-x)$(0.98K_{0.5}Na_{0.5}NbO_3$–$0.02LiTaO_3)$-x $(0.96Bi_{0.5}Na_{0.5}TiO_3$–$0.04BaTiO_3)$ piezoelectric ceramics, *Journal of the European Ceramic Society.* **28**, 16, 3193–3198, (2008).
13. Z. Yang, Y. Chang, and L. Wei, Phase transitional behavior and electrical properties of lead-free $(K_{0.44}Na_{0.52}Li_{0.04})(Nb_{0.96-x}TaxSb_{0.04})$ O_3 piezoelectric ceramics. *Applied physics letters.* **90**, 4, 042911–042911–3, (2007).
14. H. Wang, D. Ruan, Y. J. Dai *et al.* , Relationship between phase structure and electrical properties of $(K_{0.5}Na_{0.5})$ NbO_3–$LiTaO_3$lead-free ceramics. *Current Applied Physics.* **12**, 2, 504–508, (2012).

<u>แบบสรุปปิดโครงการวิจัย *(จัดทำแยกต่างหากจากรายงานฉบับสมบูรณ์)*</u>

สัญญาเลขที่ TRG5680095 **ชื่อโครงการ** การศึกษาพฤติกรรมการสับเปลี่ยนเฟร์โรอิเล็กทริกโดเมนของสาร Ta-Doped $Na_{0.5}K_{0.5}NbO_3$ เฟร์โรอิเล็กทริกปราศจากสารตะกั่ว ภายใต้สนามไฟฟ้า

หัวหน้าโครงการ ผู้ช่วยศาสตราจารย์ ดร. สุดเขตต์ พจน์ประไพ **หน่วยงาน** มหาวิทยาลัยเทคโนโลยีสุรนารี

โทรศัพท์ 044224542 **โทรสาร**.....**อีเมล์** soodkhet@g.sut.ac.th

สถานะผลงาน ☐ **ปกปิด** ☒ **ไม่ปกปิด**

ความสำคัญ / ความเป็นมา

ปัจจุยันนี้มีการค้นคว้าวิจัยวัสดุไพอิโซอิเล็กทริกปลอดสารตะกั่วกันมาอย่างต่อเนื่อง สารไพอิโซอิเล็กทริกในกลุ่มอัลคาไลน์ โพแทสเซียมโซเดียมไนโอเบต ($K_{1-x}Na_xNbO_3$: KNN) เป็นสารที่นักวิจัยเริ่มให้ความสนใจเนื่องจากมีความเป็นอันตรายต่อร่างกายและสิ่งแวดล้อมค่อนข้างต่ำอีกทั้งยังสามารถพัฒนาได้อีกมาก ด้วยการเติมสารเจือ (dopant) ลงไปเพื่อปรับปรุงสมบัติต่างๆ ไม่ว่าจะเป็น โครงสร้าง ความหนาแน่น ค่าคงที่ไดอิเล็กทริก ค่าคงที่ไพอิโซอิเล็กทริก ความสามารถในการสับเปลี่ยนทิศทางของโดเมนเฟร์รอิเล็กทริก (ferroelectric domain switchability) และ พฤติกรรมความล้าทางไฟฟ้า (electrical fatigue) ซึ่งแสดงถึงอายุการใช้งานของวัสดุนั้น ๆ

วัตถุประสงค์ของโครงการ

1 เพื่อศึกษาผลของการเติมแทนทาลัม (Ta^{5+}) ต่อสมบัติเฟร์โรอิเล็กทริกและไดอิเล็กทริกของเซรามิก KNN-LST

2 เพื่อการศึกษาพฤติกรรมการสับเปลี่ยนเฟร์โรอิเล็กทริกโดเมนของเซรามิก KNN-LST ภายใต้สนามไฟฟ้า

3 เพื่อศึกษาพฤติกรรมความล้าทางไฟฟ้าของสารโพแทสเซียมโซเดียมไนโอเบตที่เจือด้วยลิเทียม แอนติโมนี และแทนทาลัม ตามสูตร $(K_{0.50}Na_{0.46}Li_{0.04})(Nb_{(0.96-x)}Sb_{0.04}Ta_x)O_3$: KNN-LST ภายใต้สนามไฟฟ้ากระแสสลับ

ผลการวิจัย *(สั้น ๆ ที่บ่งชี้ประเด็นข้อค้นพบ กระบวนการ ผลผลิต และการเรียนรู้)*

จากผลการศึกษาดังกล่าวสามารถอธิบายถึงผลของการเติมสารเจือ Ta^{5+} ที่มีต่อพฤติกรรมความล้าทางไฟฟ้าได้ว่าการเติมสารเจือ Ta^{5+} สามารถช่วยลดการเกิดความล้าทางไฟฟ้าได้เนื่องจากการเติมสารเจือ Ta^{5+} เข้าไปในโครงสร้างของสารเซรามิก KNN-LST

ทำให้สารมีสภาพแนวโน้มแสดงลักษณะฮาร์ดเซรามิก (hard ceramic) เพิ่มขึ้นคือต้องใช้สนามไฟฟ้าที่สูงขึ้นในการทำให้เกิดโพราไรเซชัน และทำให้วงวนเกิดการอิ่มตัว การเสื่อมสภาพการมีขั้ว (depolarization) ก็จะเกิดขึ้นได้ยากกว่าซอร์ฟเซรามิก และยังพบว่าที่ 0.08 โมล นั้นเป็นปริมาณที่เหมาะสมที่สุด เมื่อเปรียบเทียบกับจากค่าโพลาไรเซชันคงค้างหลังการทดสอบความล้าทางไฟฟ้าเนื่องจากที่ปริมาณการเติมนี้มีปริมาณการลดลงน้อยที่สุดเมื่อเทียบกับสูตรอื่น

คำสืบค้น (Keywords)

. KNN-LST, Lead-free ferroelectric, Electrical fatigue, Domain orientation

การนำผลงานวิจัยไปใช้ประโยชน์ *(ดูคำจำกัดความ และตัวอย่างด้านหลังแบบฟอร์ม)*

☐ **ด้านนโยบาย** **โดยใคร** *(กรุณาให้ข้อมูลเจาะจง)*.....

มีการนำไปใช้อย่างไร

.....

.....

☐ **ด้านสาธารณะ** **โดยใคร** *(กรุณาให้ข้อมูลเจาะจง)*

มีการนำไปใช้อย่างไร

☐ **ด้านชุมชนและพื้นที่** **โดยใคร** *(กรุณาให้ข้อมูลเจาะจง)* .....

มีการนำไปใช้อย่างไร

.....

.....

☐ **ด้านพาณิชย์** **โดยใคร** *(กรุณาให้ข้อมูลเจาะจง)* .....

มีการนำไปใช้อย่างไร

.....

.....

☑ **ด้านวิชาการ** **โดยใคร** *(กรุณาให้ข้อมูลเจาะจง) งานวิจัยของสถาบันวิจัย และมหาวิทยาลัย*

มีการนำไปใช้อย่างไร *(กรุณาให้ข้อมูลเจาะจง)*

.เป็นความรู้พื้นฐานเพื่อใช้ในการผลิตเซรามิกเฟร์โรอิเล็กทริกปราศจากสารตะกั่ว

☐ **ยังไม่มีการนำไปใช้** (โปรดกรอกในกรอบถัดไป)

(กรณีที่ยังไม่มีการใช้ประโยชน์) **ผลงานวิจัยมีศักยภาพในการนำไปใช้ประโยชน์**

☐ **ด้านนโยบาย** ☐ **ด้านสาธารณะ** ☐ **ด้านชุมชนและพื้นที่** ☐ **ด้านพาณิชย์** ☐ **ด้านวิชาการ**

ข้อเสนอแนะเพื่อให้ผลงานถูกนำไปใช้ประโยชน์

.....

.....

การเผยแพร่/ประชาสัมพันธ์ *(กรุณาให้รายละเอียด พร้อมแนบหลักฐาน)*

1. สิ่งพิมพ์ หรือสื่อทั่วไป

   ☐ **หนังสือพิมพ์** ☑ **วารสาร** ☐ **โทรทัศน์** ☐ **วิทยุ** ☐ **เว็บไซต์** ☐ **คู่มือ/แผ่นพับ** ☐ **จัดประชุม/อบรม** ☐ **อื่น ๆ**

   .....

   .....

2. สิ่งพิมพ์ทางวิชาการ *(วารสาร, การประชุม ให้ระบุรายละเอียดแบบการเขียนเอกสารอ้างอิง เพื่อการค้นหาซึ่งควรประกอบด้วย ชื่อผู้แต่ง ชื่อเรื่อง แหล่งพิมพ์ ปี พ.ศ. (ค.ศ.) ฉบับที่ หน้า)*

   1. Chunmanus Uthaisar, Puripat Kantha, Rattikorn Yimnirun, **Soodkhet Pojprapai** (2012). Effect of Sintering Temperature of Lead-free $(K_{0.50}Na_{0.46}Li_{0.04})(Nb_{(0.96-x)}Sb_{0.04}Ta_x)O_3$ Ceramics on Piezoelectric Properties. Integrated Ferroelectrics. Vol.149: 114-120
   2. Thanakorn Iamsasri, Goknur Tutuncu, Chunmanus Uthaisar, **Soodkhet Pojprapai** and Jacob L. Jones (2013). Analysis methods for characterizing ferroelectric/ferroelastic domain reorientation in orthorhombic perovskite materials and application to Li-doped $Na_{0.5}K_{0.5}NbO_3$. Journal Materials Science. Vol. 48: 6905-6910

Analysis methods for characterizing ferroelectric/ferroelastic domain reorientation in orthorhombic perovskite materials and application to Li-doped $Na_{0.5}K_{0.5}NbO_3$

Thanakorn Iamsasri, Goknur Tutuncu, Chunmanus Uthaisar, Soodkhet Pojprapai & Jacob L. Jones

Journal of Materials Science
Full Set - Includes `Journal of Materials Science Letters'

ISSN 0022-2461
Volume 48
Number 20

J Mater Sci (2013) 48:6905-6910
DOI 10.1007/s10853-013-7495-2

Springer

J Mater Sci (2013) 48:6905–6910
DOI 10.1007/s10853-013-7495-2

Analysis methods for characterizing ferroelectric/ferroelastic domain reorientation in orthorhombic perovskite materials and application to Li-doped $Na_{0.5}K_{0.5}NbO_3$

Thanakorn Iamsasri · Goknur Tutuncu · Chunmanus Uthaisar · Soodkhet Pojprapai · Jacob L. Jones

Received: 4 April 2013 / Accepted: 31 May 2013 / Published online: 11 June 2013

Abstract Ferroelectric and ferroelastic domains can be reoriented during the application of electric field through domain wall motion. This study develops a method to quantify the domain reorientation in perovskite ferroelectrics with orthorhombic crystal lattices. In situ, high-energy X-ray diffraction was utilized to obtain intensity ratios that are necessary for the calculation. Domain reorientation in orthorhombic Li-doped $Na_{0.5}K_{0.5}NbO_3$ is then quantified using this method. The preference of domain orientations is explained by considering the angle between spontaneous polarization of the respective domains and the applied electric field direction. The extent of domain reorientation increases as the Li substitution increases which additionally correlates to increased piezoelectric coefficient d_{33} and field-induced strain. Increased domain wall motion is further proposed to originate due to the increased compositional proximity to the morphotropic phase boundary, a proposed universal behavior in ferroelectric compositions-containing phase boundaries.

Electronic supplementary material The online version of this article (doi:10.1007/s10853-013-7495-2) contains supplementary material, which is available to authorized users.

T. Iamsasri · G. Tutuncu · J. L. Jones (✉)
Department of Materials Science and Engineering, University of Florida, Gainesville, FL 32611, USA
e-mail: jjones@mse.ufl.edu

C. Uthaisar · S. Pojprapai
School of Ceramic Engineering, Institute of Engineering, Suranaree University of Technology, Nakorn Ratchasima 30000, Thailand

Introduction

Ferroelectrics are used in many applications and devices ranging from ferroelectric memories to high-strain actuators [1, 2]. In situ measurements of domain wall motion in ferroelectric materials have been provided by electro-optic imaging microscopy, X-ray microdiffraction, and X-ray diffraction from polycrystalline materials [3–7]. One benefit of X-ray diffraction is that intensities can be used to quantify the degree of preferred domain orientation and is thus able to measure changes in non-180° domain volume fractions during and after applied fields [4, 8–10]. Methods have been developed for transforming intensities of ferroelastic degenerate peaks into domain volume fractions in tetragonal and rhombohedral perovskites [4, 8–10]. Though domain wall motion in orthorhombic perovskite materials (i.e., space group *Amm*2) has been described qualitatively, however, quantitative relationships between intensities and domain volume fractions have not yet been developed for these materials [11]. Materials that exhibit this space group, such as $Na_{0.5}K_{0.5}NbO_3$ (NKN), have been rigorously investigated in a resurgence of research on lead-free materials and quantitative methods to describe domain wall motion are needed [12, 13].

The piezoelectric properties of $Na_yK_{1-y}NbO_3$ are maximum at approximately $y = 0.5$ [14]. In 2004, Saito et al. [15] highlighted the abilities of NKN solid solutions to achieve high-piezoelectric properties relative to lead-based ferroelectrics. The properties of unmodified NKN typically include a piezoelectric coefficient, d_{33}, of approximately 160 pC/N and a planar coupling coefficient, k_p, of 0.45 [14]. By doping with a certain amount of Li, the structure can be transformed from orthorhombic to tetragonal at room temperature, and the piezoelectric properties are enhanced near the morphotropic phase boundary

(MPB) [16]. The MPB of $(1-x)(Na_{0.5}K_{0.5})NbO_3$–$xLiNbO_3$ ($100x$LNKN) occurs between $x = 0.05-0.07$ [17]. The phase diagram of LNKN has been reported by Klein et al. [18].

This study develops a method to quantify the domain wall motion for orthorhombic ferroelectrics and applies the method to LNKN with compositions $x = 0.03-0.05$. Due to the proximity of these compositions to the MPB, a significant amount of domain wall motion is expected. The amount of domain wall motion as a function of Li content supports a hypothesis that Li enhances properties of NKN such as d_{33} through an increase in domain wall motion. This suggests that domain wall motion strongly affects the electromechanical behavior of LNKN.

Experiment

LNKN samples were prepared by a conventional mixed oxide method. The starting substances were powders of Nb_2O_5 (Sigma-Aldrich Co. 99.9 % purity), Na_2CO_3 (Sigma-Aldrich Co. 99.9 % purity), K_2CO_3 (Merck, 99 % purity), and $LiCO_3$ (Merck, 98.5 % purity). The powders were mixed with zirconia ball-milling media in ethanol for 24 h. The mixture was dried at 180 °C for 2 h. The dried mixture was ground and sieved to reduce the mixture particle size and screen the rough particles. The powder was calcined at 850 °C for 24 h. To prepare the green body, the powder was mixed with polyvinyl alcohol 5 vol% aqueous solution as an organic binder. After mixing, the rough particles of powder were screened again by using a 120 mesh sieve. Then, the fine powder was formed into a disk by using a uniaxial hydraulic pressing machine at 130 MPa and cold isostatic pressing machine at 250 MPa. The samples were sintered at 1190 °C with the heating rate of 5 °C/min in air for 2 h. The sintered LNKN specimens were successively polished using 800, 1200, 1800, and 2000 grit size SiC grinding papers. The samples were cut to approximate dimensions of 1.21 × 1 × 0.8 mm^3, and after annealing at 600 °C for 4 h, they were gold sputtered and coated with silver electrode on opposing parallel surfaces. The density of all samples is more than 90 % of the theoretical density. The average grain size is about 1–2 μm. The phase purity of samples is confirmed by X-ray diffraction.

Diffraction patterns were measured during the application of electric fields using high-energy X-rays at beamline 11-ID-C of the Advanced Photon Source, Argonne National Laboratory. The X-ray beam had a wavelength of 0.10798 Å and size of 0.5 × 0.5 mm. The diffraction patterns were measured in forward scattering geometry using a Perkin Elmer area detector at a distance of approximately 2250 mm. The samples were subjected to an electric field amplitude of 2 kV/mm utilizing a triangular bipolar waveform with a frequency of 0.125 Hz. The amplitude of electric field was increased to 2.5 kV/mm for a second cycle. The field amplitudes of both cycles are above the coercive field of LNKN.

Results and discussion

The structure of $100x$LNKN, where $0 < x < 5$, can be described by using an orthorhombic or pseudo-monoclinic reference frame (the latter of which involves lattice parameters $a_M = c_M$). The equivalent plane indices for certain reflections of these two reference frames are listed in Table 1. The possible polarization axes in orthorhombic perovskite materials are in the $\langle 110 \rangle_M$ directions, where M indicates the pseudo-monoclinic cell, as shown in Fig. 1, [19]. Recently, Ge et al. [20] have shown that 5LNKN may have a monoclinic structure which is different from the pseudo-monoclinic structure that equally describes the orthorhombic phase. The structure reported by Ge et al. includes an additional lattice distortion of the perovskite structure involving the expansion of lattice parameter a_M and the contraction of lattice parameter c_M so that $a_M \neq c_M$. Reference to the pseudo-monoclinic unit cell (M) in this study hereafter refers to the former definition, in which $a_M = c_M$. The quantification and analysis of the degree of domain reorientation in monoclinic crystal structures are complicated since the monoclinic unit cell has an infinite number of possible polarization directions. For simplicity, therefore, we develop equations in this study for the orthorhombic case which may, in certain instances, apply equally to pseudo-monoclinic unit cells. To confirm the different levels of Li substitution, the lattice parameters of relevant LNKN compositions with respect to the orthorhombic reference frame are calculated from the X-ray diffraction patterns and are shown in Table 2.

For orthorhombic LNKN, the spontaneous polarization vector is parallel to the c-direction of the unit cell. The diffracting planes reported in this study are approximately perpendicular to the applied electric field. When the electric field is applied, the domains reorient such that the domain orientations with polarization vectors most closely parallel to the electric field are preferred relative to the

Table 1 Indices for $\{220\}_M$ reflections with respect to pseudo-monoclinic and orthorhombic reference frame

Pseudo-monoclinic	Orthorhombic	2θ (degrees)	d-Spacing (Å)
$(202)_M$	$(004)_O$	4.36	1.42
$(022)_M$	$(400)_O$	4.39	1.41
$(220)_M$	$(222)_O$	4.41	1.40

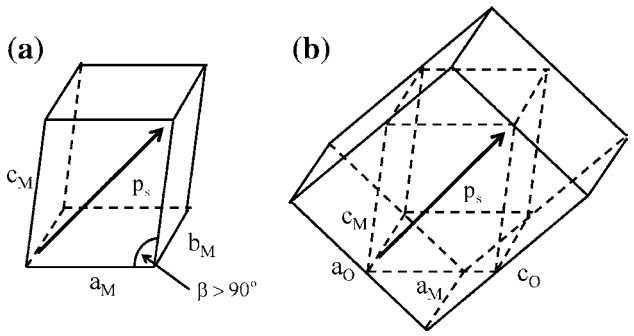

Fig. 1 Spontaneous polarization direction in orthorhombic LNKN with respect to **a** pseudo-monoclinic cell and **b** orthorhombic unit cell

Table 2 Lattice parameters of LNKN with respect to orthorhombic reference frame

Composition	a (Å)	b (Å)	c (Å)
3LNKN	5.644	3.945	5.679
4LNKN	5.644	3.942	5.680
5LNKN	5.640	3.941	5.679

other domain orientations. Domain reorientation is therefore expected to be measurable in the $\{hh0\}_M$ reflections because they correspond to domains with polarization axes parallel and perpendicular to the electric field direction. However, for orthorhombic LNKN, the $\{110\}_M$ reflections are only clearly split into two measurable peaks which are insufficient to quantify the degree of domain reorientation between three variants. The $\{220\}_M$ reflections, which are parallel to the $\{110\}_M$ reflections, split into three resolved peaks because of larger peak splitting at higher 2θ angles. Thus, the $\{220\}_M$ reflections are used to quantify the domain reorientation in this study.

The vertical sector of two-dimensional X-ray diffraction patterns, which measures scattering vectors approximately parallel to the electric field direction, was integrated by Fit2d software using ±7.5° azimuthal angles [3, 4]. Figure 2 shows the $\{220\}_M$ reflections with crystallographic poles parallel to the electric field direction during the application of triangular bipolar waveform with amplitude 2 kV/mm and time period 80 s on unpoled 3LNKN, 4LNKN, and 5LNKN. The intensity change in the $\{220\}_M$ reflections with applied electric field indicates the changes in non-180° domain volume fractions. At an electric field amplitude of approximately 1.5 kV/mm, the intensity of the $(202)_M$ reflection increases while the intensity of the $(220)_M$ reflection decreases significantly. The integrated intensity of individual $\{220\}_M$ reflections was obtained by fitting the measured intensity profile to three symmetric Gaussian functions with a constraint that the $(022)_M$ reflection and the $(220)_M$ reflection have the same full width at half maximum. This constraint was found to be necessary to enable reliable convergence of the fit and is justified on the basis that microstructural and instrumental broadening should not be significantly different for these diffraction peaks. Figure 3 shows representative data measured at a field amplitude of 2 kV/mm, including the measured intensity, the component Gaussian profile fits, the overall fit, and the difference between the measured and overall fit.

In 1957, Subbarao et al. [8] developed an equation to quantify the reorientation of domains in tetragonal $BaTiO_3$ under applied stress, and several authors have since quantified the domain switching in tetragonal and rhombohedral structures under applied electric field using similar formulae [4, 9, 10]. However, quantification methods of domain reorientation for orthorhombic perovskite materials have not been developed. This study presents a quantification method leading to a value called the *fraction of domain interchange*, the detailed derivation of which can be found in the supplementary material. The intensity from domain orientations corresponding to any of the diffraction peaks can change to other peaks during the application of electric field. The intensity changes can be used to determine the fraction of domain interchange from peak i to peak j (n_{i-j}). For orthorhombic perovskite materials, n_{i-j} for the $\{220\}_M$ reflections is defined as

$$n_{i-j} = \frac{-R_i + R_j}{R_{202} + R_{022} + R_{220}}, \quad (1)$$

where $i, j = 202$, 022, or 220, $i \neq j$, and R_i is the ratio of integrated intensity during application of electric field to integrated intensity of the peak i from the unpoled sample. The fraction of domain interchange scales from −1 to 1, and n_{i-j} is equal to $-n_{j-i}$. If the value of n_{i-j} is positive, the domains corresponding to peak i reorient to domains corresponding to peak j.

Using this method, Fig. 4 shows the fraction of domain interchange for 3LNKN, 4LNKN, and 5LNKN during the application of a triangular bipolar waveform of amplitude 2.5 kV/mm and time period 80 s. The fraction of domain interchange is hysteretic because of the irreversible motion of domain walls. From Fig. 4, $n_{022-202}$ and $n_{220-202}$ values are positive while $n_{220-022}$ is negative. These results indicate that the domains corresponding to the $(022)_M$ reflection reorient to the domains corresponding to the $(202)_M$ reflection and the $(220)_M$ reflection, while domains corresponding to the $(220)_M$ reflection reorient to the domains corresponding to the $(202)_M$ reflection. These results agree qualitatively with the diffraction patterns shown in Fig. 2, which show that the intensity of $(202)_M$ increases and the intensity of $(022)_M$ decreases after application of electric field. After the electric field is applied, the domains can be listed from the most to the least preferred orientation as follows: $(202)_M$, $(220)_M$, and $(022)_M$.

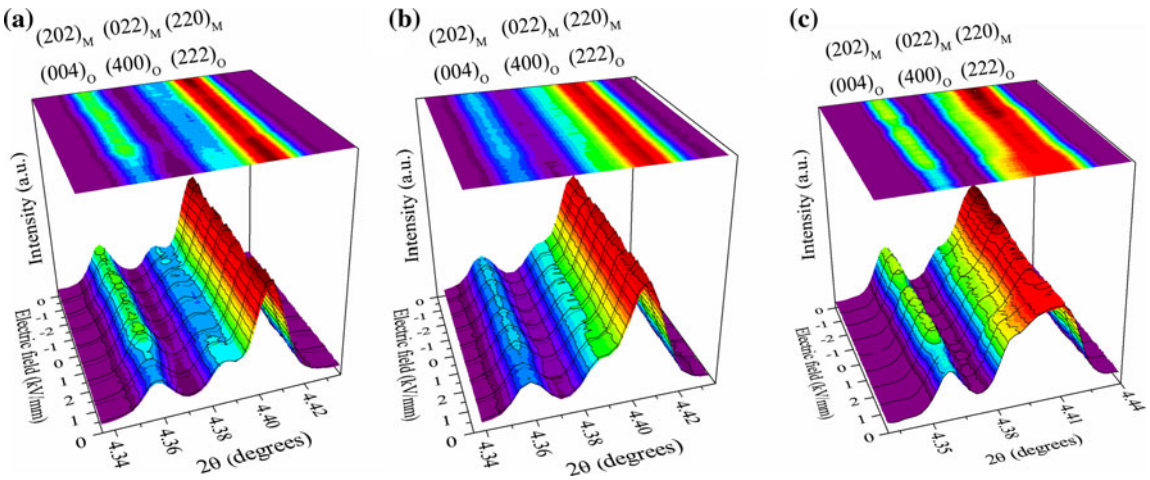

Fig. 2 The $\{220\}_M$ reflections with crystallographic poles parallel to the electric field direction during the first application of triangular bipolar waveform on unpoled **a** 3LNKN, **b** 4LNKN, and **c** 5LNKN samples

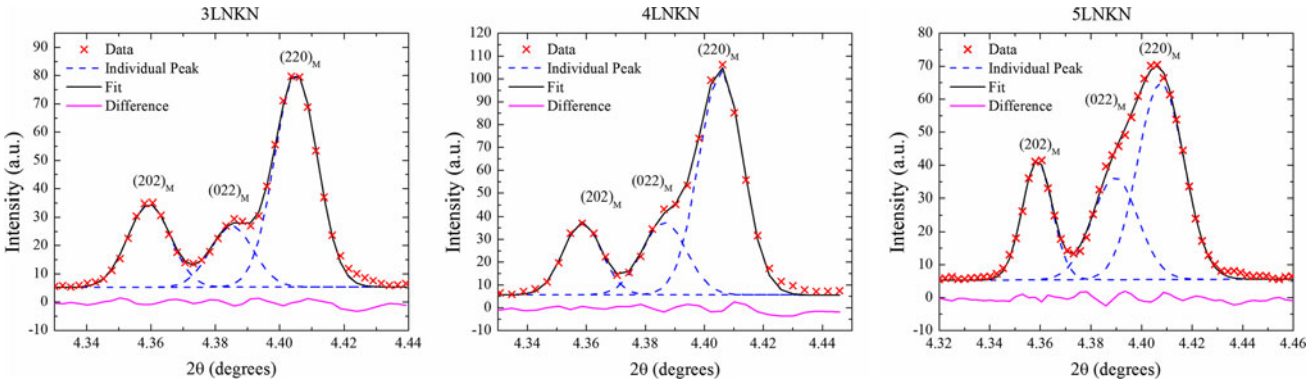

Fig. 3 Measured intensity, Gaussian profile fits, the overall fit, and difference between the measured and overall fit of $\{220\}_M$ reflections of 3LNKN, 4LNKN, and 5LNKN at 2 kV/mm

The lattice parameters of orthorhombic NKN have been reported as $a_O = 5.6395$ Å, $b_O = 3.9399$ Å, and $c_O = 5.6725$ Å and are nearly constant in the range $x = 0-0.05$ [17, 21]. The lattice parameters of the corresponding pseudo-monoclinic cell are $a_M = c_M = 4.000$ Å, $b_M = 3.940$ Å, and $\beta = 90.34°$. The possible polarization axes are in the $\langle 110 \rangle_M$ directions of a pseudo-monoclinic cell where the spontaneous polarization vector is parallel to c_O as shown in Fig. 1. Figure 5 shows the spontaneous polarization vectors for each plane of the $\{220\}_M$ reflections. In this study, the applied electric field is always approximately perpendicular to the diffracting planes, but the spontaneous polarization directions are different for each domain. The spontaneous polarization vector and the applied electric field are parallel in the domains corresponding to the $(202)_M$ plane, perpendicular in the domains corresponding to the $(022)_M$ plane, and at a 60.34° angle in the domains corresponding to the $(220)_M$ plane. After the electric field is applied, the domains reorient to have polarization vector as closely as possible to the electric field. This means that the domains corresponding to the $(202)_M$ reflection are the most preferred, the $(220)_M$ reflection are the second most preferred, and the $(002)_M$ reflection are the least preferred. The measured intensities correspond to this expectation based on the angle between the polarization direction and the applied electric field direction.

Results from Lai et al. and Wang et al. [13, 22] showed that d_{33} and field-induced strain of LNKN increase as Li content increases for $x = 0-0.06$. From Fig. 4, it can be seen that the values of fraction of domain interchange (n_{i-j}) also increase as Li content increases. Thus, domain wall motion can be considered as one of the possible mechanisms, which enhances the field-induced strain of LNKN. It should be noted that the domain wall motion during application of low-frequency or static electric fields of strong amplitude is strictly a distinctly different loading scenario from domain wall motion during application of cyclic, weak-electric field amplitudes such as those applied during measurement of piezoelectric properties. However,

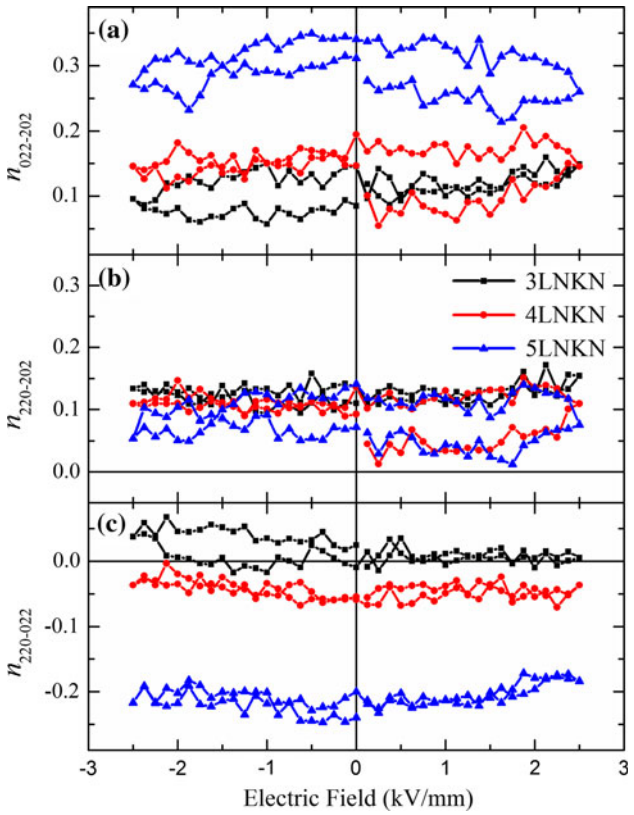

Fig. 4 Fraction of domain interchange of 3LNKN, 4LNKN, and 5LNKN during the application of triangular bipolar waveform with amplitude 2.5 kV/mm and time period 80 s

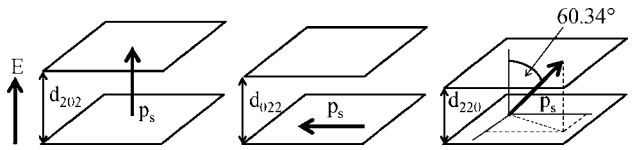

Fig. 5 Schematic of spontaneous polarization vectors in the $\{220\}_M$ planes

a high degree of domain wall motion during application of strong-electric fields is typically related to high mobility of domain walls during subcoercive field application, e.g., as observed in donor-modified lead zirconate titanate in which a large contribution of domain wall displacement to field-induced strain and piezoelectric coefficients is observed [23]. Thus, the increase in domain wall motion observed during application of high-electric fields in this study may be correlated with an equivalent enhancement in domain wall contributions to the piezoelectric coefficients. The degree of domain wall motion during electrical poling has also been previously correlated with enhanced piezoelectric coefficients in other ferroelectric ceramic materials, e.g., as has reported in orthorhombic-structured Aurivillius phases [24]. In this study, the substantial increase of domain wall motion seen with Li substitution may be considered to be due to either a fundamental change in the way in which the substituent (i.e., Li) interacts with domain walls, or the movement of the composition closer to the MPB. In considering the first possibility (substituents interacting with domain walls), we note that Li substitution in NKN is isovalent and it is not expected to generate other point defects to compensate for charge. Thus, Li substitution is dissimilar to acceptor and donor doping which are common approaches to modify domain wall mobility and generate hard and soft ferroelectric behavior in Pb-based perovskites. It is therefore unlikely that Li or any other newly generated defect substantially affects the mobility or pinning of domain walls. We therefore return to the possibility that Li substitution enhances domain wall motion by changing the compositional proximity to the phase boundary. In $PbZr_xTi_{1-x}O_3$ (PZT), it has been shown that domain wall motion increases as the MPB is approached [23]. Thus, the enhancement in domain reorientation that is observed in LNKN with increasing Li concentration may also be considered to be due to increased compositional proximity to the phase boundary. This result provides additional evidence for an emerging universality in perovskite ferroelectric materials that domain wall motion increases with increasing proximity to phase boundaries.

Conclusions

This study presents a method to quantify domain switching in orthorhombic structured materials that lead to a value called fraction of domain interchange. The method is applied to several orthorhombic compositions of Li-substituted NKN ferroelectric materials. The domains corresponding to the $(202)_M$ reflections were found to be the most preferred during electric field application, the domains corresponding to the $(220)_M$ reflections were found to be the second most preferred, and the domains corresponding to the $(022)_M$ reflections were found to be the least preferred. The preference of domain orientations is explained by the angle between the spontaneous polarization in each domain and the electric field direction. The fraction of domain interchange increases as Li content increases, which corresponds to higher d_{33} and field-induced strain. The fact that domain wall motion increases significantly by Li substitution is attributed to the increasing compositional proximity to the phase boundary with increasing Li concentration.

Acknowledgements JJ acknowledges support for this study from the Army Research Office through W911NF-09-1-0435. TI acknowledges support from the Development and Promotion of Science and Technology Talents Project, Royal Thai Government. SP would like to acknowledge the Thai Research Fund (TRF) MRG56 and Synchrotron Light Research Institute (Public Organization),

Thailand for support of this project. Use of the Advanced Photon Source, an Office of Science User Facility operated for the US Department of Energy (DOE) Office of Science by Argonne National Laboratory, was supported by the US DOE under Contract No. DE-AC02-06CH11357.

References

1. Scott JF, Paz de Araujo CA (1989) Science 246:1400
2. Park SE, Shrout TR (1997) J Appl Phys 82:1804
3. Tutuncu G, Damjanovic D, Chen J, Jones JL (2012) Phys Rev Lett 108:177601
4. Pramanick A, Daniels JE, Jones JL (2009) J Am Ceram Soc 92:2300
5. Gopalan V, Mitchell TE (1999) J Appl Phys 85:2304
6. Grigoriev A, Do DH, Kim DM, Eom CB, Adams B, Dufresne EM, Evans PG (2006) Phys Rev Lett 96:187601
7. Pojprapai S, Russell J, Man H, Jones JL, Daniels JE, Hoffman M (2009) Acta Mater 57:3932
8. Subbarao EC, McQuarrie MC, Buessem WR (1957) J Appl Phys 28:1194
9. Bedoya C, Muller C, Baudour JL, Madigou V, Anne M, Roubin M (2000) Mater Sci Eng B 75:43
10. Jones JL, Slamovich EB, Bowman KJ (2005) J Appl Phys 97:034113
11. Hall DA, Azough F, Middleton-Stewart N, Cernik RJ, Freer R, Mori T, Kungl H, Curfs C (2010) Funct Mater Lett 03:31
12. Tutuncu G, Chang Y, Poterala S, Messing GL, Jones JL (2012) J Am Ceram Soc 95:2653
13. Lai F, Li JF, Zhu ZX, Xu Y (2009) J Appl Phys 106:064101
14. Jaeger RE, Egerton L (1962) J Am Ceram Soc 45:209
15. Saito Y, Takao H, Tani T, Nonoyama T, Takatori K, Homma T, Nagaya T, Nakamura M (2004) Nature 432:84
16. Guo Y, Kakimoto KI, Ohsato H (2004) Appl Phys Lett 85:4121
17. Sun X, Deng J, Chen J, Sun C, Xing X (2009) J Am Ceram Soc 92:3033
18. Klein N, Hollenstein E, Damjanovic D, Trodahl HJ, Setter N, Kuball M (2007) J Appl Phys 102:014112
19. Jaffe B, Cook WR, Jaffe H (1971) Piezoelectric Ceramics. Academic, New York
20. Ge W, Ren Y, Zhang J, Devreugd CP, Li J, Viehland D (2012) J Appl Phys 111:103503
21. Wu L, Zhang JL, Wang CL, Li JC (2008) J Appl Phys 103:084116
22. Wang K, Li JF (2007) Appl Phys Lett 91:262902
23. Pramanick A, Damjanovic D, Daniels JE, Nino JC, Jones JL (2011) J Am Ceram Soc 94:293
24. Jones JL, Slamovich EB, Bowman KJ, Lupascu DC (2005) J Appl Phys 98:104102